Inorganic Chemistry

Article

pubs.acs.org/IC

# Near-Infrared Luminescence and Color Tunable Chromophores Based on $Cr^{3+}$-Doped Mullite-Type $Bi_2(Ga,Al)_4O_9$ Solid Solutions

Chengyin Liu,[†,‡] Zhiguo Xia,[*,†] Mingyue Chen,[†] Maxim S. Molokeev,[§,∥] and Quanlin Liu[†]

[†]School of Materials Sciences and Engineering, University of Science and Technology Beijing, Beijing 100083, China

[‡]School of Materials Sciences and Technology, China University of Geosciences, Beijing 100083, China

[§]Laboratory of Crystal Physics, Kirensky Institute of Physics, SB RAS, Krasnoyarsk 660036, Russia

[∥]Department of Physics, Far Eastern State Transport University, Khabarovsk, 680021 Russia

Supporting Information

**ABSTRACT:** $Cr^{3+}$-activated mullite-type $Bi_2Ga_{(4-x)}Al_xO_9$ ($x$ = 0, 1, 2, 3, and 4) solid solutions were prepared by the solid state reaction, and their spectroscopic properties were investigated in conjunction with the structural evolution. Under excitation at 610 nm, $Bi_2[Ga_{(4-y)}Al_y]_{3.97}O_9$:0.03$Cr^{3+}$ ($y$ = 0, 1, 2, 3, and 4) phosphors exhibited broad-band near-infrared (NIR) emission peaking at ~710 nm in the range 650−850 nm, and the optimum $Cr^{3+}$ concentrations and concentration quenching mechanism were determined. Except for the interesting NIR emission, the body color changed from white (at $x$ = 0) to green (at $x$ = 0.08) for $Bi_2Ga_{4-x}O_9$:$xCr^{3+}$, and from light yellow (at $x$ = 0) to deep brown (at $x$ = 0.08) for $Bi_2Al_{4-x}O_9$:$xCr^{3+}$, respectively. Moreover, as a result of variable Al/Ga ratio, the observed body color for $Bi_2[Ga_{(4-y)}Al_y]_{3.97}O_9$:0.03$Cr^{3+}$ ($y$ = 0, 1, 2, 3, and 4) varied from deep brown to green. The relationship between the observed colors and their diffuse reflectance spectra were also studied for the understanding of the different absorption bands. The results indicated that $Cr^{3+}$-doped $Bi_2Ga_{(4-x)}Al_xO_9$ solid solutions appeared as the bifunctional materials with NIR phosphors and color-tunable pigments.

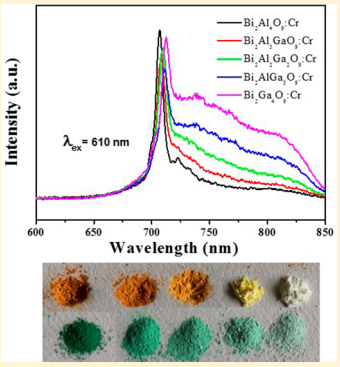


## 1. INTRODUCTION

The optical properties of $Cr^{3+}$ appearing as substitutional impurities have been extensively studied in many hosts, and the structural information and some insight into to coupling of the ion with the environment can be found from such studies.[1,2] Recently, the gallium and aluminum oxides activated by the $Cr^{3+}$ ion have been reported as the new promising deep-red and near-infrared (NIR) emission materials and color-stable inorganic pigments. The observed spectroscopic properties were related with the spin-forbidden $^4T_2 \rightarrow {}^4A_2$ transition of $Cr^{3+}$ for the narrow-band emissions at 700 nm, spin-allowed $^2E \rightarrow {}^4A_2$ transition of $Cr^{3+}$ for a broad-band emission (650−1600 nm), and Ga−O or Al−O charge-transfer transition for the color tunable chromophores, respectively.[3,4] Therefore, $Cr^{3+}$ doped gallates/aluminates materials have demonstrated potential applications as luminescent solar concentrator to convert the ultraviolet or visible light into the deep-red or NIR light.[5] Moreover, persistent NIR luminescence has been recently reported in several $Cr^{3+}$-doped gallogermanates compounds.[6] It was also found that persistent NIR luminescence originating from the $Cr^{3+}$-contained compounds have great potential for *in vivo* bioimaging because of no need for *in situ* excitation, high signal-to-noise ratio, and deep tissue penetration.[7,8] Except for this, the hue of the intense, bright green and yellow body colors can be controlled by the choice of the $Cr^{3+}$ doped gallates/aluminates compounds. As we know, most pigments with different colors are based on the light absorption that is separated by an amount of energy corresponding to the visible portion of the spectrum.[9] Furthermore, the resulting colors are not from electronic transitions but from structural features. Several examples of structure-induced visible light emission can also be found in inorganic materials. Their color hue can be finely tuned by the concentration of doped elements and the compositions of the hosts.[10−12] Herein, $Cr^{3+}$-doped gallates/aluminates compounds can act as both the NIR/deep-red phosphors and the color tunable pigments owing to the $Cr^{3+}$ chromophores at gallium and aluminum sites in the suitable hosts.

In this Article, the two end members of isostructural bismuth gallate/aluminate, $Bi_2Ga_4O_9$ and $Bi_2Al_4O_9$, as well as their solid solutions of $Bi_2Ga_{(4-y)}Al_yO_9$ ($y$ = 1, 2 and 3) were prepared, where the $Cr^{3+}$ is doped to partially substitute the $Ga^{3+}/Al^{3+}$ sites equally. The photoluminescence properties of $Cr^{3+}$ in these hosts and the corresponding diffuse reflectance spectra were characterized. The $Bi_2M_4O_9$ compounds (M = Al, Ga) belong to orthorhombic system with space group *Pbam*. The bonding environment of the $Bi^{3+}$ ion is strongly anisotropic with three strong and one weaker Bi2−O bonds on one side, and the lone electron pair on the other.[13] In the structure of $Bi_2M_4O_9$, $Bi^{3+}$ atoms are 6-fold coordinated to form six-vertex polyhedral $BiO_6$, and the $M^{3+}$ cations exist in two type sites

**Received:** November 20, 2014
**Published:** January 26, 2015






DOI: 10.1021/ic502779d
*Inorg. Chem.* 2015, 54, 1876−1882

with both tetrahedral and octahedral coordinations. Similar to the sillimanite and mullite structures, chains of edge-sharing $MO_6$ octahedra run parallel to the *c*-axis. The octahedral chains of $MO_6$ are linked via pairs of corner-sharing $MO_4$ tetrahedra, forming $M_2O_7$ dimers, which are arranged in *ab* planes and alternate with planes of $BiO_4$ groups along the *c* axis.[14] Our present study pays attention to the substitution of $Ga^{3+}$ or $Al^{3+}$ or small amount of $Cr^{3+}$ at $M^{3+}$ sites, which cause the color change. The relationship between the crystal structure and the spectroscopic properties of $Cr^{3+}$ in these hosts were investigated in detail, and the relationship between the observed colored pigments and diffuse reflectance spectra have also been determined.

## 2. EXPERIMENTAL SECTION

A series of $Cr^{3+}$-doped $Bi_2Ga_{(4-y)}Al_yO_9$ ($y$ = 0, 1, 2, 3, and 4) solid solution samples were synthesized by the high temperature solid state reaction. The starting materials were $Bi_2O_3$ (99.95%), $Ga_2O_3$ (99.95%), $Al_2O_3$ (99.995%), and $Cr_2O_3$ (99.995%), which were used directly without any treatment. The raw materials were weighed stoichiometrically, and the above powder reactants were mixed and ground thoroughly in an agate mortar. The comparative experimental results indicated that the phase formation temperature keeps invariable for $Cr^{3+}$-doped $Bi_2Ga_{(4-y)}Al_yO_9$ ($y$ = 0, 1, 2, 3, and 4) solid solution depending on the different Ga/Al ratio, and additional flux is unnecessary. Therefore, the mixtures were sintered at 1000 °C for 5 h in air atmosphere; after this, the samples were furnace-cooled to room temperature, and the samples were finally obtained.

X-ray diffraction (XRD) patterns were collected using X-ray diffraction (SHIMADZU, XRD-6000) with Cu K$\alpha$ radiation ($\lambda$ = 0.154 06 nm) at 40 kV, 30 mA. The powder diffraction data were refined by using TOPAS 4,[15] the step size of 2$\theta$ was 0.016°, and the counting time was 5 s per step. Photoluminescence excitation (PLE) and emission (PL) spectra were performed by using fluorescence spectrophotometer (F-4600, HITACHI, Japan) equipped with a photomultiplier tube operating at 400 V, and a 150 W Xe lamp used as the excitation lamp. The decay curves were recorded on a spectrofluorometer (HORIBA, JOBIN YVON FL3-21), and the 370 nm pulse laser radiation (spectra-LED) was used as the excitation source. Diffuse reflection spectrum was recorded by a UV−vis−NIR spectrophotometer (SHIMADZU UV-3600) by using the white powder $BaSO_4$ as a reference standard.

## 3. RESULTS AND DISCUSSION

XRD patterns of the as-prepared $Cr^{3+}$-doped $Bi_2Ga_{4-y}Al_yO_9$ ($y$ = 0, 1, 2, 3, and 4) solid solution samples were checked to verify the phase purity, as shown in Figure 1a. All of the diffraction peaks of the samples can be basically indexed to the corresponding standard data for the two end members of the orthorhombic phases of $Bi_2Ga_4O_9$ (ICSD card no 76-2240) and $Bi_2Al_4O_9$ (ICSD card no 83-1995), suggesting that this series of $Bi_2Ga_{4-x}Al_xO_9$ ($x$ = 0, 1, 2, 3, 4) solid solution samples with different Ga/Al ratios can form a single phase, and a small amount of $Cr^{3+}$ also will not change the phase structure. In the meantime, with increasing $Al^{3+}/Ga^{3+}$ ratio, all the diffraction peaks shift to higher 2$\theta$ angles. This could be more obvious in Figure 1b, where the plane (001) moves to higher angle from bottom to top. It implies the regular shrinkage of lattice cell according to Bragg's law ($2d \sin\theta = n\lambda$, where $d$ is the spacing between the planes in the atomic lattice, and $\theta$ is the angle between the incident ray and the scattering planes, $n$ is an integer, $\lambda$ is the wavelength of incident X-ray).[16] This variation also verified the formation of the continuous solid solution of $Bi_2Ga_{4-y}Al_yO_9$ via the Al/Ga substitution.

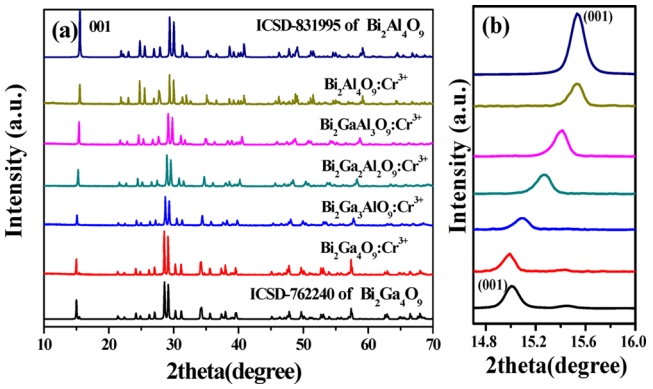


**Figure 1.** (a) XRD patterns of as-prepared $Cr^{3+}$-doped $Bi_2Ga_{4-y}Al_yO_9$ ($y$ = 0, 1, 2, 3, and 4) samples, and the standard data for $Bi_2Ga_4O_9$ (ICSD card no 76-2240) and $Bi_2Al_4O_9$ (ICSD card no 83-1995) are shown as the reference. (b) The zoom-in XRD patterns of $Bi_2Ga_{4-y}Al_yO_9$ samples in the range 14.2−16° for (001) diffraction peaks.

In order to further check the phase composition and crystal structure of this series of solid solution samples, the powder diffraction data of $Bi_2Ga_{4-y}Al_yO_9$ ($y$ = 0, 1, 2, 3, and 4) samples for Rietveld analysis were collected. Almost all peaks were indexed by orthorhombic cell (*Pbam*) with parameters close to $Bi_2Al_4O_9$, $Bi_2Ga_4O_9$, or $Bi_2Fe_2Ga_2O_9$. Therefore, crystal structures of $Bi_2Al_4O_9$ and $Bi_2Ga_4O_9$ were used as the initial model for the two end members, and $Bi_2Fe_2Ga_2O_9$ was taken as starting model of the three intermediate compositions for Rietveld refinement.[14,17] It is considered that the sites of Al ion in $Bi_2Al_4O_9$ were occupied by Al and Ga ions, and their occupations were refined. When more Ga ions were introduced into the $Bi_2Al_4O_9$ matrix, the Ga ion preferred to occupy the Al2 sites to form a tetrahedron. Refinements were stable and gave low *R*-factors, as shown in Table 1. The Rietveld refinement results on the Rietveld plots of the five $Bi_2Ga_{4-y}Al_yO_9$ ($y$ = 0, 1, 2, 3, and 4) samples were given in the Supporting Information, and the corresponding crystallographic information files (CIF) were also presented in the Supporting Information.

As further given in Figure 2a, the lattice parameters *a*, *b*, *c*, and *V* of this series of solid solution samples decrease according to Végard's law. The linear behavior of the cell volume of the solid solution samples per Al content ($y$) (Figure 2a) suggests that the Ga ions were successfully incorporated into the structure of $Bi_2Al_4O_9$ according to the designed chemical formula. The Al1/Ga1 site forms in tetrahedron with coordination number of 4, and the Al2/Ga2 site forms in octahedron with coordination number of 6. Furthermore, the ion radii of $Al^{3+}$ and $Ga^{3+}$ with coordination number of 4 and 6 are 0.39, 0.47 Å, and 0.535, 0.62 Å, respectively. The ion radius of $Cr^{3+}$ with 6 coordination is 0.615 Å.[18] On the basis of the ion radius and coordination analysis, we suggest that the doped $Cr^{3+}$ ions will occupy the Al2/Ga2 sites since $Cr^{3+}$ ions prefer to lie in the octahedral sites, forming the $CrO_6$ octahedron in the $Bi_2Ga_{(4-y)}Al_yO_9$ ($y$ = 0, 1, 2, 3, 4) solid solution samples. Accordingly, the crystal structure of the $Bi_2Al_4O_9$ compound is illustrated in Figure 2b. The unit cell contains two formula units. Half of all $Al^{3+}$ ions are tetrahedrally coordinated, and the other half are octahedrally coordinated, as highlighted in Figure 2c. The bismuth ions are 4-fold coordinated to form four-vertex polyhedron $BiO_4$. The octahedral chains of $AlO_6$ are linked via pairs of corner-sharing $AlO_4$ tetrahedra, forming $Al_2O_7$ dimers,


DOI: 10.1021/ic502779d
Inorg. Chem. 2015, 54, 1876−1882

**Table 1. Main Parameters of Refinement Processing and the Corresponding Results of the $Bi_2Ga_{(4-x)}Al_xO_9$ Solid Solution Samples**

| | $Bi_2Al_4O_9$ | $Bi_2Al_3GaO_9$ | $Bi_2Al_2Ga_2O_9$ | $Bi_2AlGa_3O_9$ | $Bi_2Ga_4O_9$ |
|---|---|---|---|---|---|
| space group | *Pbam* | *Pbam* | *Pbam* | *Pbam* | *Pbam* |
| *a*, Å | 7.724 91(7) | 7.7792(2) | 7.836 53(18) | 7.893 43(12) | 7.929 74(7) |
| *b*, Å | 8.115 68(6) | 8.1620(2) | 8.209 98(18) | 8.261 81(12) | 8.305 09(7) |
| *c*, Å | 5.698 22(5) | 5.742 91(17) | 5.795 06(14) | 5.855 09(9) | 5.898 19(5) |
| *V*, Å$^3$ | 357.238(5) | 364.637(19) | 372.842(15) | 381.834(10) | 388.438(5) |
| *Z* | 2 | 2 | 2 | 2 | 2 |
| 2$\theta$-interval, deg | 10−120 | 10−120 | 10−120 | 10−120 | 10−120 |
| no. reflns | 300 | 306 | 311 | 320 | 326 |
| no. params of refinement | 97 | 62 | 49 | 50 | 52 |
| $R_{wp}$, % | 7.76 | 9.44 | 8.57 | 7.32 | 6.82 |
| $R_p$, % | 5.88 | 6.83 | 6.17 | 5.01 | 5.18 |
| $R_{exp}$, % | 3.07 | 2.99 | 3.21 | 3.09 | 2.92 |
| $\chi^2$ | 2.53 | 3.16 | 2.67 | 2.37 | 2.33 |
| $R_B$, % | 4.17 | 3.15 | 2.18 | 1.85 | 1.07 |

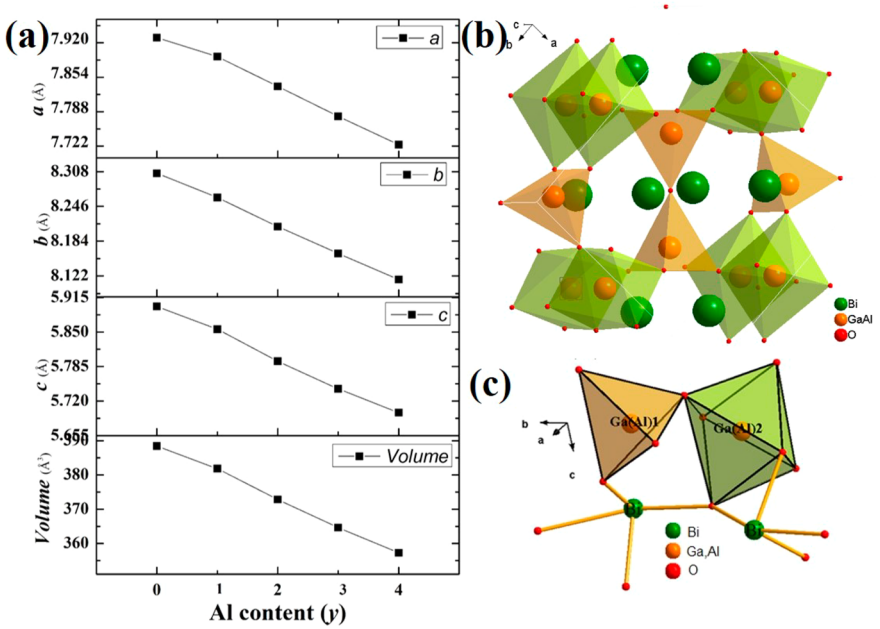


**Figure 2.** (a) Variation of unit cell parameters (*a*, *b*, *c*, and *V*) of $Cr^{3+}$ doped $Bi_2Ga_{4-y}Al_yO_9$ ($y$ = 0, 1, 2, 3, and 4) solid solution samples showing a linear decrease following Végard's law dependent on increasing Al content ($y$). (b) Crystal structure of $Bi_2Al_4O_9$ viewed along the *c* axis. The $AlO_4$ tetrahedra and $AlO_6$ octahedra are highlighted in the unit cell, and the $Bi_2Ga_4O_9$ is isostructural with $Bi_2Al_4O_9$. (c) The bonding of $O^{2-}$ anions with $Bi^{3+}$ and $Al^{3+}$ cations in the indepentent part of the $Bi_2$ (Ga, Al)$_4O_9$ unit cell.

and via highly asymmetric $BiO_4$ groups.[13,14] In order to discuss the occupation of the $Cr^{3+}/Al^{3+}$ substitution details in the present $Bi_2Ga_{4-y}Al_yO_9$ ($y$ = 0, 1, 2, 3, and 4) samples, the fractional atomic coordinates and occupancies of them obtained by the Rietveld refinement have been given in Table S1 in the Supporting Information. One can see that the concentrations of Ga in Al2 site are corresponding to 1, 0.819, 0.635, 0.372, and 0; as a comparison, the concentrations of Ga in Al1 site are 1, 0.681, 0.365, 0.128, 0 for $y$ = 0, 1, 2, 3, 4, respectively. So, we can think that the Ga ion preferred to occupy the Al2 sites when more Ga ions were introduced into the $Bi_2Al_4O_9$ matrix. Furthermore, it is believed that the emission of $Cr^{3+}$ in solid solution compounds $Bi_2Ga_{4-y}Al_yO_9$ ($y$ = 0, 1, 2, 3, 4) intuitively correlates to contraction of lattice volumes with the $Cr^{3+}/Al^{3+}$ substitution, as shown in Figure 2a. As the atom number per cell keeps constant, the decrease of lattice volume means the shortening of distance between atoms. This enhances the interaction between atoms, so $Cr^{3+}$ will experience a stronger crystal field as the content of Al increases.

Figure 3,b shows the photoluminescence excitation (PLE) and emission (PL) spectra of the selected $Bi_2Ga_{3.97}O_9$:0.03$Cr^{3+}$ and $Bi_2Al_{3.97}O_9$:0.03$Cr^{3+}$ samples, respectively. Under excitation at about 618 nm, $Bi_2Ga_{3.97}O_9$:0.03$Cr^{3+}$ exhibits a broadening $^2E \rightarrow {}^4A_2$ emission band peaking at about 710 nm that superimposes on a broad background emission ranging from ~600 to ~850 nm, as given in Figure 3a. The broadening of the $^2E \rightarrow {}^4A_2$ emission is possibly caused by the electron−phonon coupling in the host system. The PLE spectrum monitored at about 711 nm covers a very broad spectral region (from 200 to 700 nm). It consists of three main excitation bands originating from the d−d inner transitions of $Cr^{3+}$, which include the 300 nm dual-band originating from the $^4A_2 \rightarrow {}^4T_1$ ($te^2$) transition, the 438 nm band originating from the $^4A_2 \rightarrow {}^4T_1$ ($t^2e$) transition, and the 610 nm band originating from the $^4A_2 \rightarrow$



DOI: 10.1021/ic502779d
*Inorg. Chem.* 2015, 54, 1876−1882

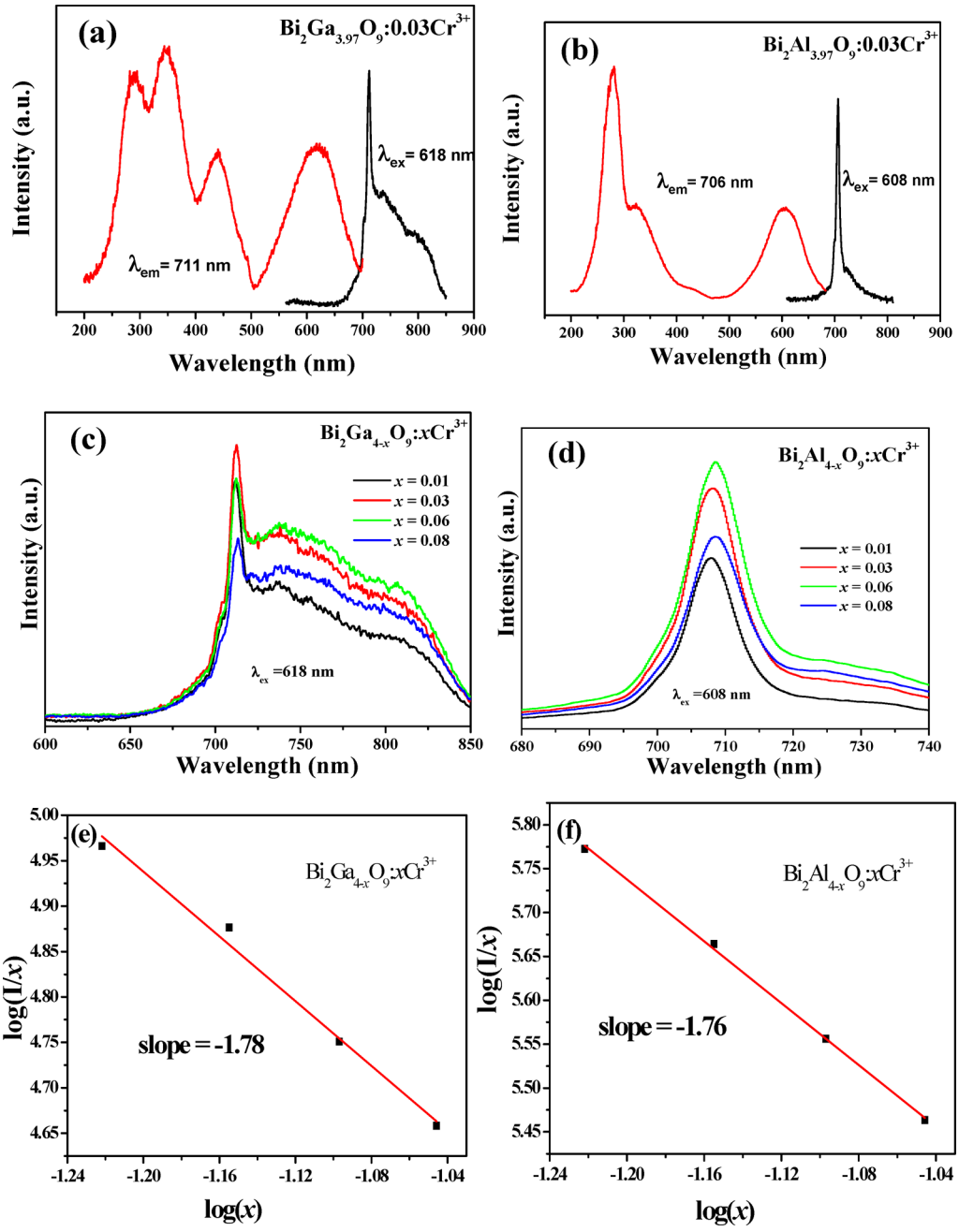


**Figure 3.** (a) PLE ($\lambda_{em}$ = 711 nm) and PL ($\lambda_{ex}$ = 618 nm) spectra of the selected $Bi_2Ga_{3.97}O_9$:0.03$Cr^{3+}$ sample. (b) PLE ($\lambda_{em}$ = 706 nm) and PL ($\lambda_{ex}$ = 608 nm) spectra of the selected $Bi_2Al_{3.97}O_9$:0.03$Cr^{3+}$ sample. $Cr^{3+}$ concentration dependent PL spectra of $Bi_2Ga_{4-x}O_9$:$xCr^{3+}$ (c) and $Bi_2Al_{4-x}O_9$:$xCr^{3+}$ (d) phosphors. The relationships of lg($x$) versus lg($I/x$) in $Bi_2Ga_{4-x}O_9$:$Cr^{3+}$ (e) and $Bi_2Al_{4-x}O_9$:$Cr^{3+}$ (f) phosphors.

$^4T_2(t^2e)$ transition. It is believed that an intertransition from $Cr^{3+}$ ground state to conduction band ($^4A_2 \rightarrow$ CB) at around 350 nm was overlapped with the $^4A_2 \rightarrow {}^4T_1$ ($te^2$) transition.[19] As a comparison, we can find a similar spectral profile in Figure 3b for the PLE and PL spectra of the selected $Bi_2Al_{3.97}O_9$:0.03$Cr^{3+}$ sample. However, the PL spectral width of $Bi_2Al_{3.97}O_9$:0.03$Cr^{3+}$ is obviously smaller than that of $Bi_2Ga_4O_9$:$Cr^{3+}$, and the PLE spectral intensity of $Bi_2Al_{3.97}O_9$:0.03$Cr^{3+}$ is also slightly weaker than that of $Bi_2Ga_{3.97}O_9$:0.03$Cr^{3+}$, which will be discussed later. Figure 3c,d shows the $Cr^{3+}$ concentration dependent PL spectra of $Bi_2Ga_{4-x}O_9$:$xCr^{3+}$ and $Bi_2Al_{4-x}O_9$:$xCr^{3+}$ phosphors ($x$ = 0.01, 0.03, 0.06, and 0.08 mol %). The emission spectra have no obvious changes in the spectra configuration except for the emission intensity. The emission intensity at 711 nm in $Bi_2Ga_{4-x}O_9$:$xCr^{3+}$ reaches a saturation point at $x$ = 0.03. However, the emission intensity from 725 to 850 nm reaches a saturation point at $x$ = 0.06. As a comparison, $Cr^{3+}$ concentration ($x$) in $Bi_2Al_{4-x}O_9$:$xCr^{3+}$ reaches a saturation point at $x$ = 0.06 in the full range of the observed PL spectrum.

In order to further understand the photophysical mechanism on the concentration quenching for the two end members of $Bi_2Ga_{4-x}O_9$:$xCr^{3+}$ and $Bi_2Al_{4-x}O_9$:$xCr^{3+}$ phosphors, the interaction type between the doped activators ($Cr^{3+}$) can be calculated by the following equation[20,21]

$$\frac{I}{x} = K[1 + \beta(x)^{\theta/3}]^{-1} \quad (1)$$



DOI: 10.1021/ic502779d
Inorg. Chem. 2015, 54, 1876−1882

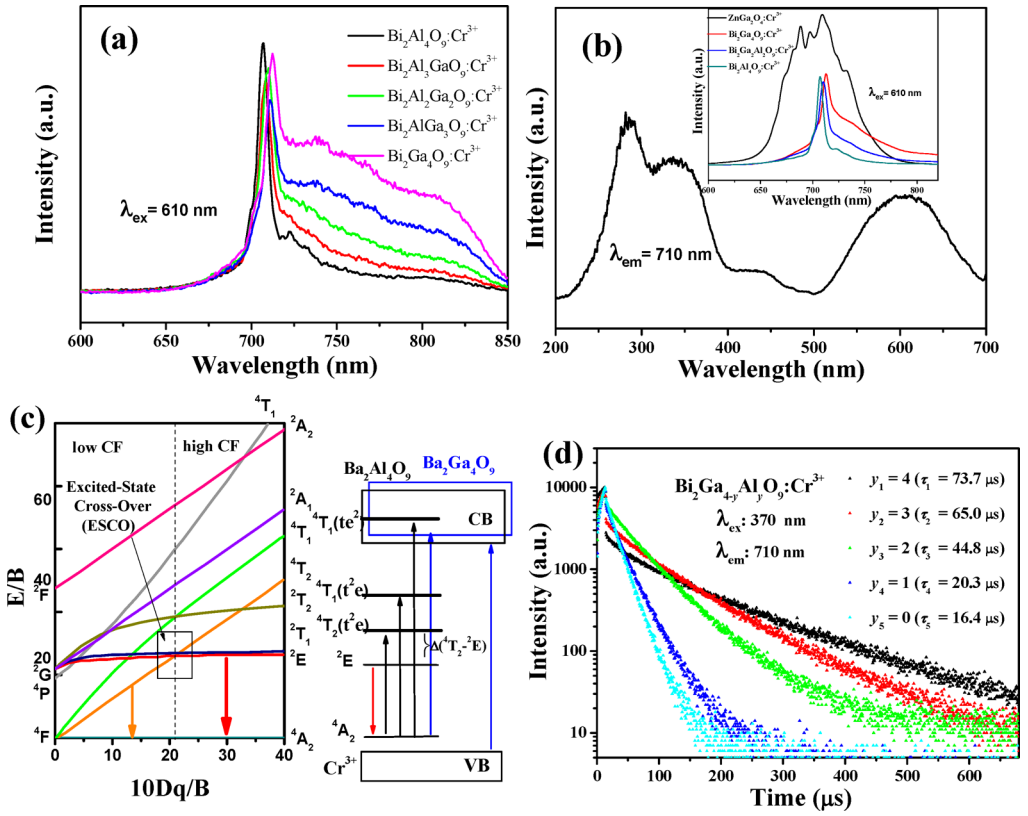


**Figure 4.** (a) Al content dependent PL spectra of $Bi_2[Ga_{4-y}Al_y]_{3.97}O_9{:}0.03Cr^{3+}$ ($y$ = 0, 1, 2, 3, and 4) phosphors ($\lambda_{ex}$ = 610 nm). (b) PLE spectrum of the selected $Bi_2[Ga_2Al_2]_{3.97}O_9{:}0.03Cr^{3+}$ phosphor ($\lambda_{em}$ = 710 nm), and the inset shows the comparison of the PL spectra of the $ZnGa_2O_4{:}Cr^{3+}$ phosphor and the selected $Bi_2(Ga,Al)_4O_9{:}Cr^{3+}$ solid solution phosphors. (c) Tanabe–Sugano diagram and energy level diagram for $Cr^{3+}$ in $Bi_2[Ga_{4-y}Al_y]_{3.97}O_9{:}0.03Cr^{3+}$ phosphors. (d) Al concentration dependent decay curves and the corresponding lifetime values of $Bi_2[Ga_{4-y}Al_y]_{3.97}O_9{:}0.03Cr^{3+}$ phosphors.

where $x$ is the concentration of the activator ions beyond the quenching concentration, $I$ is the integral emission intensities, $K$ and $\beta$ are constants for a given sample, and $\theta$ is a function of multipole–multipole interaction. The value of $\theta$ is calculated to be 6, 8, or 10 corresponding to dipole–dipole (d–d), dipole–quadrupole (d–q), or quadrupole–quadrupole (q–q) interactions, respectively. In general, the dependence of log $(I/x)$ on log $(x)$ can yield a straight line with a slope equal to $-\theta/3$, so we can obtain a correct $\theta$ value. As shown in Figure 3e,f, the slope of the straight line $(-\theta/3)$ was found to be −1.78 and −1.76 for $Cr^{3+}$ in $Bi_2Ga_{4-x}O_9$ and $Bi_2Al_{4-x}O_9$ phosphors, respectively. So, the value of $\theta$ can be calculated as 5.79 and 5.28, which are close to 6, meaning that the dipole–dipole interaction is the dominant concentration quenching mechanism in the $Bi_2Ga_{4-x}O_9{:}Cr^{3+}$ and $Bi_2Al_{4-x}O_9{:}Cr^{3+}$ phosphors.

Figure 4a shows the Al content dependent PL spectra of $Bi_2[Ga_{4-y}Al_y]_{3.97}O_9{:}0.03Cr^{3+}$ ($y$ = 0, 1, 2, 3, and 4) phosphors. As seen from the PL spectra, the emission intensity of broad band (assigned to $^4T_2$–$^4A_2$ transition) from 710 to 850 nm increases with increasing $Ga^{3+}$ concentration upon the fixed $Cr^{3+}$ content, which can be ascribed to the reduced site symmetry around $Cr^{3+}$ ions caused by the disorder.[3−5] The coexistence of the narrow-line emission and broad-band emission in the observed PL spectra suggests that part of $Cr^{3+}$ ions locate in a high crystal field site when $Ga^{3+}$ substituted $Al^{3+}$ completely in the present isostructural $Bi_2M_4O_9$ host. Figure 4b shows the typical PLE spectrum for the intermediate component, $Bi_2[Ga_2Al_2]_{3.97}O_9{:}0.03Cr^{3+}$ phosphor. It is found this PLE spectrum is similar as that of the $Bi_2Ga_{3.97}O_9{:}0.03Cr^{3+}$ phosphor. Moreover, we have also compared the PL spectra of the well-known $ZnGa_2O_4{:}Cr^{3+}$ phosphor and the selected $Bi_2(Ga,Al)_4O_9{:}Cr^{3+}$ solid solution phosphors under the same excitation wavelength. It is found that the PL intensity of $ZnGa_2O_4{:}Cr^{3+}$ phosphor is obviously stronger than that of the $Bi_2(Ga,Al)_4O_9{:}Cr^{3+}$ phosphors, which should be related with the intrinsic character of the different crystal structure and the coordination environment of $Cr^{3+}$ in a different host. In order to further investigate this Al content dependent variation of the PL spectra, Figure 4c gives a Tanabe–Sugano diagram and the corresponding energy level diagram, which could be used to describe a complete level scheme for $Cr^{3+}$.[15] Each excited state exhibits a rather different PL because of the different electron–lattice coupling. The spin-allowed $^4T_2$–$^4A_2$ transition, whose energy corresponds to the crystal field (CF) splitting, Δ, is strongly coupled to the lattice providing short-lived broadband PL. Nevertheless the spin-forbidden $^2E$–$^4A_2$ transition does not involve any change in electronic configuration and is therefore weakly coupled to the lattice, giving rise to long-lived narrow-line emission. It is known that the two distinct luminescence behaviors are depending on the crystal field: (1) broad band emission ($^4T_{2g}$–$^4A_{2g}$) for 10Dq < $10Dq_{ESCO}$ in the high crystal field sites (ESCO means the excited state cross over), and narrow ruby-like emission ($^2E_g$–$^4A_{2g}$) for 10Dq > $10Dq_{ESCO}$ in the low crystal field sites.[22,23] The difference of the PL emission behaviors for the $Bi_2[Ga_{4-y}Al_y]_{3.97}O_9{:}0.03Cr^{3+}$ ($y$ = 0, 1, 2, 3, and 4) phosphors is also related to the Al concentration dependent decay behaviors. It is found that the lifetime values


DOI: 10.1021/ic502779d
Inorg. Chem. 2015, 54, 1876−1882

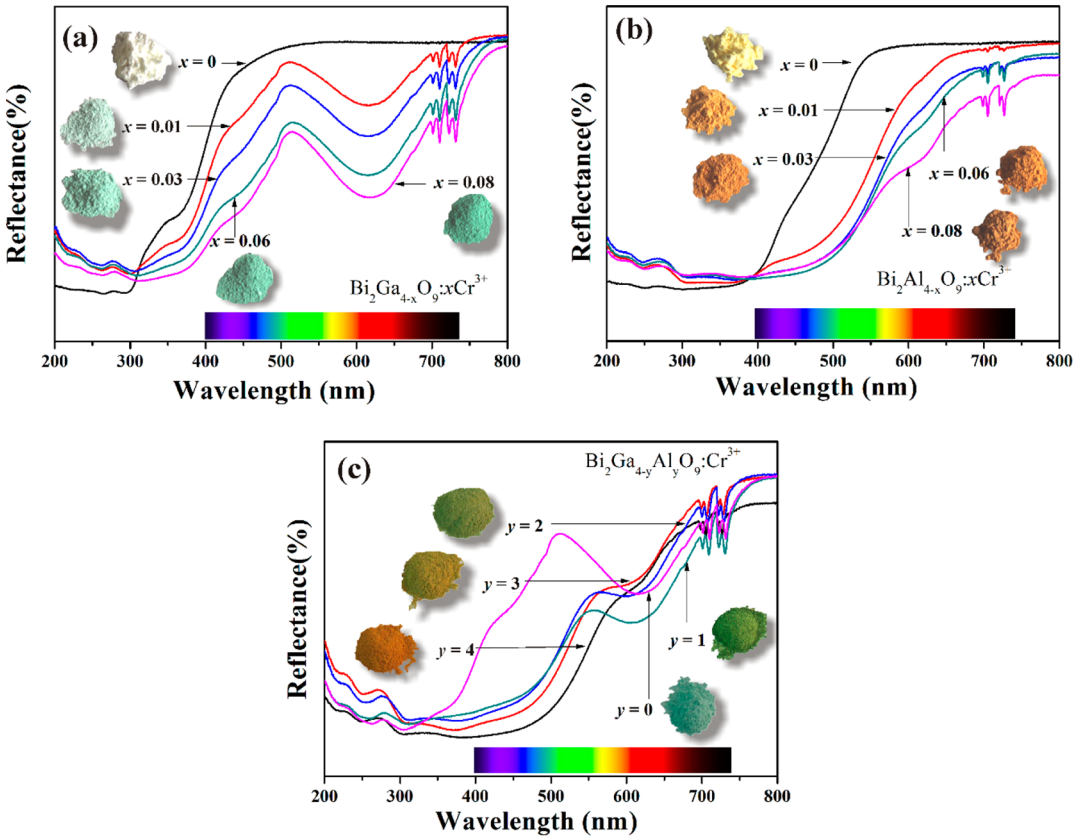


**Figure 5.** Diffuse reflectance spectra and the corresponding colors for the $Bi_2Ga_{4-x}O_9:xCr^{3+}$ (a), $Bi_2Al_{4-x}O_9:xCr^{3+}$ (b), and $Bi_2[Ga_{4-y}Al_y]_{3.97}O_9:0.03Cr^{3+}$ (c) samples.

of the decay curves for the $Bi_2[Ga_{4-y}Al_y]_{3.97}O_9:0.03Cr^{3+}$ phosphors are 16.4, 20.3, 44.8, 65.0, and 73.7 $\mu$s, respectively, when the Al contents in the host are corresponding to $y$ = 0, 1, 2, 3, and 4 and the $Cr^{3+}$ concentration stays invariable. That is to say, the lifetime values increased with increasing Al content from the end members $Bi_2Ga_{3.97}O_9:0.03Cr^{3+}$ to $Bi_2Al_{3.97}O_9:0.03Cr^{3+}$ sample, which means that $Cr^{3+}$ ions possess the short lifetime when occupying a high crystal field site in the $Bi_2Ga_4O_9$ host.

As a kind of interesting solid solution phosphors with NIR emission, the thermal quenching behaviors of this series of phosphors have also been investigated, and the temperature dependent PL spectra of $Cr^{3+}$-doped $Bi_2Ga_{4-y}Al_yO_9$ ($y$ = 0, 1, 2, 3, and 4) samples (Supporting Information Figure S6) are given in the Supporting Information. The results indicated that the emission intensities for all the $Cr^{3+}$-doped $Bi_2Ga_{4-y}Al_yO_9$ ($y$ = 0, 1, 2, 3, and 4) samples decreased with increasing temperature. However, the emission peaks and spectral profiles stay invariable indicating the better NIR color stability at high temperature.

Except for the interesting NIR emission that originated from the $Cr^{3+}$ in the different crystal field environment of the present $Bi_2M_4O_9$ compounds, the body color of the samples drew much attention, which means that they can also act as the pigment materials with bifunctional applications.[24] Therefore, the diffuse reflectance spectra and the corresponding colors for the as-prepared $Bi_2Ga_{4-x}O_9:xCr^{3+}$, $Bi_2Al_{4-x}O_9:xCr^{3+}$, $Bi_2[Ga_{4-y}Al_y]_{3.97}O_9:0.03Cr^{3+}$ samples are shown in Figure 5a–c. As for the $Bi_2Ga_4O_9$ and $Bi_2Al_4O_9$ hosts, the color of the pigments can be adjusted by different $Cr^{3+}$ content. For example, since $Cr^{3+}$ is substituted for $Ga^{3+}$, the body color changed from white (at $x$ = 0) to green (at $x$ = 0.08) for $Bi_2Ga_{4-x}O_9:xCr^{3+}$. As we can find from the diffuse reflectance spectra in Figure 5a, there is no absorption in the visible region, and the color is white at $x$ = 0. Green color can be observed with the introduction of $Cr^{3+}$ at $Ga^{3+}$ sites, and the color originates from additional optical absorption at the low-energy regions of the visible spectrum, which is mainly due to an Cr–O charge-transfer transition and some allowed transition of $Cr^{3+}$ corresponding to some sharp lines near 730 nm.[25,26] As for $Bi_2Al_{4-x}O_9:xCr^{3+}$, the color varied from light yellow (at $x$ = 0) to deep brown (at $x$ = 0.08). It is found that absorption edge of $Bi_2Al_4O_9$ is relatively near to visible region at 550 nm compared to the 450 nm for $Bi_2Ga_4O_9$. Furthermore, the optical absorption at the high-energy region overlaps for the Al–O and Cr–O charge-transfer transitions (Figure 5b), so that the deep brown color can be observed. The absorption intensity in the corresponding region increased with increasing Cr content for this two end members. Moreover, as a result of variable Al content, the observed colors for $Bi_2[Ga_{4-y}Al_y]_{3.97}O_9:0.03Cr^{3+}$ ($y$ = 0, 1, 2, 3, and 4) varied from deep brown to green as discussed above. There were two obvious strong broad absorption bands and some sharp absorption lines in the 400–800 nm range, and the absorption intensity in this region increased with increasing Ga content (Figure 5c). The high energy peak is mainly due to the Al–O and Ga–O charge-transfer transition, and there is also a contribution from Cr–O charge transfer that results in a low-energy shoulder which has sharp lines, and both factors affect the observed color. There is interesting spectral evolution, and the observed body colors made them act as the good pigments for the potential applications.



DOI: 10.1021/ic502779d
*Inorg. Chem.* 2015, 54, 1876–1882

## 4. CONCLUSIONS

In summary, $Cr^{3+}$-activated mullite-type $Bi_2Ga_{(4-x)}Al_xO_9$ ($x$ = 0, 1, 2, 3, and 4) solid solutions were reported in this Article, and the structral evolution, NIR photoluminescence properties, and the correlation between the observed colors and the diffuse reflectance spectra were studied in detail. The present materials can act as the potential NIR phosphors, the sharp NIR emission peaking at ~710 nm can be obseved for all the samples, and the emission bands in the range 650−850 nm for $Bi_2[Ga_{4-y}Al_y]_{3.97}O_9$:$0.03Cr^{3+}$ ($y$ = 0, 1, 2, 3, and 4) phosphors were enhanced owing to the substitution of $Ga^{3+}$ by $Al^{3+}$. Obvious body color evolution can be also found from white (at $x$ = 0) to green (at $x$ = 0.08) for $Bi_2Ga_{4-x}O_9$:$xCr^{3+}$, and from light yellow (at $x$ = 0) to deep brown (at $x$ = 0.08) for $Bi_2Al_{4-x}O_9$:$xCr^{3+}$, respectively. Moreover, $Bi_2[Ga_{4-y}Al_y]_{3.97}O_9$:$0.03Cr^{3+}$ ($y$ = 0, 1, 2, 3, and 4) varied from deep brown to green with increasing Al content. The relationship between the observed colors and their diffuse reflectance spectra was also studied. The above results indicated that this series of compounds can be also used as functional inorganic pigments.

## ■ ASSOCIATED CONTENT

### Supporting Information

Rietveld plots of the $Bi_2Ga_{4-y}Al_yO_9$ ($y$ = 0, 1, 2, 3, and 4) solid solution samples and the corresponding crystallographic information files (CIF), temperature dependent PL spectra, and the relative emission intensities under different temperature of $Cr^{3+}$ doped $Bi_2Ga_{4-y}Al_yO_9$ ($y$ = 0, 1, 2, 3, and 4) samples. This material is available free of charge via the Internet at http://pubs.acs.org.

## ■ AUTHOR INFORMATION

### Corresponding Author

* E-mail: xiazg@ustb.edu.cn. Phone: +86-10-8237-7955. Fax: +86-10-8237-7955.

### Notes

The authors declare no competing financial interest.

## ■ ACKNOWLEDGMENTS

The present work was supported by the National Natural Science Foundations of China (Grants 51002146, 51272242), Natural Science Foundations of Beijing (2132050), the Program for New Century Excellent Talents in University of Ministry of Education of China (NCET-12-0950), Beijing Nova Program (Z131103000413047), Beijing Youth Excellent Talent Program (YETP0635), the Funds of the State Key Laboratory of New Ceramics and Fine Processing, Tsinghua University (KF201306), and Fundamental Research Funds for the Central Universities (FRF-TP-14-005A1).

## ■ REFERENCES

(1) Van Schaik, W.; Poort, S.; Blasse, G.; Omil, J. A. P.; Marquez, S. B. *Chem. Mater.* **1994**, *6*, 755−760.
(2) Deren, P. J.; Watras, A.; Gagor, A.; Pazik, R. *Cryst. Growth Des.* **2012**, *12*, 4752−4757.
(3) Mitsuo, Y.; Peter, I. M.; Brian, H.; Keith, H.; Hideo, T.; Taturu, Y.; Minoru, F. *J. Phys.: Condens. Matter* **1997**, *9*, 569−578.
(4) Peter, I. M.; Brian, H.; Keith, H.; Marek, G. *J. Phys.: Condens. Matter* **1996**, *8*, 3933−3946.
(5) Liu, P. J.; Liu, J.; Zheng, X.; Luo, H. D.; Li, X. Q.; Yao, Z. L.; Yu, X. B.; Shi, X. M.; Hou, B. H.; Xia, Y. S. *J. Mater. Chem. C* **2014**, *2*, 5769−5777.
(6) Chen, D. Q.; Chen, Y.; Lu, H. W.; Ji, Z. G. *Inorg. Chem.* **2014**, *53*, 8638−8645.
(7) Abdukayum, A.; Chen, J. T.; Zhao, Q.; Yan, X. P. *J. Am. Chem. Soc.* **2013**, *135*, 14125−14133.
(8) Singh, S. K. *RSC Adv.* **2014**, *4*, 58674−58698.
(9) Merikhi, J.; Jungk, H. O.; Feldmann, C. *J. Mater. Chem.* **2000**, *10*, 1311−1314.
(10) Mizoguchi, H.; Sleight, A. W.; Subramanian, M. A. N *Inorg. Chem.* **2011**, *50*, 10−12.
(11) Tamilarasan, S.; Sarma, D.; Reddy, M. L. P.; Natarajan, S. *RSC Adv.* **2013**, *3*, 3199.
(12) Rusakov, D. A.; Belik, A. A.; Kamba, S.; Savinov, M.; Nuzhnyy, D.; Kolodiazhnyi, T.; Yamaura, K.; Takayama-Muromachi, E.; Borodavka, F.; Kroupa, J. *Inorg. Chem.* **2011**, *50*, 3559.
(13) Niizeki, N.; Wachi, M. *Z. Kristallogr.* **1968**, *127*, 173−187.
(14) Abrahams, I.; Bush, A. J.; Hawkes, G. E.; Nunes, T. *J. Solid State Chem.* **1999**, *147*, 631−636.
(15) Bruker AXS. *TOPAS V4: General Profile and Structure Analysis Software for powder Diffraction Data—User's Manual*; Bruker AXS: Karlsruhe, Germany, 2008.
(16) Smallman, R. E. *Modern Physical Metallurgy*, 4th ed.; Butterworths: London, 1985.
(17) Giaquinta, D. M.; Papaefthymiou, G. C.; Davis, W. M.; Zur Loye, H. C. *J. Solid State Chem.* **1992**, *99*, 120−133.
(18) Shannon, R. D. *Acta. Crystallogr., Sect. A* **1976**, *32*, 751−767.
(19) Zhou, J.; Xia, Z. G. *RSC Adv.* **2014**, *4*, 46313−46318.
(20) Blasse, G. *Phys. Lett. A* **1968**, *28*, 444−445.
(21) Chen, X.; Xia, Z. G.; Liu, Q. L. *Dalton Trans.* **2014**, *43*, 13370−13376.
(22) Ye, S.; Zhou, J. J.; Wang, S. T.; Hu, R. X.; Wang, D. P.; Qiu, J. R. *Opt. Express* **2013**, *21*, 4167−4173.
(23) Zhuang, Y. X.; Ueda, J.; Tanabe, S. *J. Mater. Chem. C* **2013**, *1*, 7849−7855.
(24) Weckhuysen, B. M.; Wachs, I. E.; Schoonheydt, R. A. *Chem. Rev.* **1996**, *96*, 3327−3350.
(25) Thauern, H.; Glaum, R. *Inorg. Chem.* **2007**, *46*, 2057−2066.
(26) Li, Y. Q.; Mei, S. G.; Byon, Y. J.; Wang, J. L.; Zhang, G. L. *ACS Sustainable Chem. Eng.* **2014**, *2*, 318−321.


DOI: 10.1021/ic502779d
*Inorg. Chem.* 2015, 54, 1876−1882